STRAIN-GAGE LOADS CALIBRATION PARAMETRIC STUDY†

William A. Lokos*, Rick Stauf**
***NASA Dryden Flight Research Center, ****Spiral Technology Inc.**

Keywords: *calibration parametric study, loads calibration optimization, loads calibration test, loads test design, strain-gage calibration*

Abstract

This paper documents a parametric study of various aircraft wing-load test features that affect the quality of the resultant derived shear, bending-moment, and torque strain-gage load equations. The effect of the following on derived strain-gage equation accuracy are compared: single-point loading compared with distributed loading, variation in applied test load magnitude, number of applied load cases, and wing-box-only compared with control-surface loading.

The subject of this study is an extensive wing-load calibration test of the Active Aeroelastic Wing F/A-18 airplane. Selected subsets of the available test data were used to derive load equations using the linear regression method. Results show the benefit of distributed loading and the diminishing-return benefits of test load magnitudes and number of load cases. The use of independent check cases as a quality metric for the derived load equations is shown to overcome blind extrapolating beyond the load data used to derive the load equations.

1 Introduction

Structural load measurement obtained from aircraft in flight has been depended upon for many decades for research and safety-of-flight. This measurement involves the installation of strain gages on the primary load paths and the calibration of these sensors through the application of known loads. Load equations are derived from the post-test analysis of these recorded applied loads and the strain-gage output data [1]. These load equations are then used to interpret subsequent strain-gage outputs when the applied loads are not otherwise known—such as in flight. The accuracy of these load-equation-calculated flight loads is subject to many variables, the bulk of which can be grouped into three categories:

1. the design of the strain-gage installation,
2. the design and performance of the applied-load test, and
3. the strain-gage load equation derivation process.

The focus of this paper is the design of the applied-load test. The three major questions to be answered are:

1. Which features of a strain-gage calibration load test have a significant relationship with the accuracy of the resultant load equations? Designers of such tests need an understanding of the relative merit of the various testing options in order to design a test that will produce the required quality of output while considering schedule time and cost constraints and avoiding subjecting the airframe to unnecessary risk of damage.
2. If testing the structure to a higher applied load is better than testing to a lesser load—how much load will suffice?
3. If a greater number of independent applied-load cases is better than fewer cases—how many load cases will suffice?

This research effort addresses these and similar questions.

The origin of the database for these parametric studies is the strain-gage load calibration test of the Active Aeroelastic Wing [AAW] F/A-18 aircraft, performed at the NASA Dryden Flight Research Center Flight Loads Laboratory [2] in 2001. The AAW aircraft, shown in figure 1, is the test bed for the AAW project [3, 4], which seeks to explore the use of wing elastic twist for roll control. The primary structure and flight control system of the aircraft were modified for that goal, and the structure heavily instrumented. Because the AAW project requires full exploitation of wing strength, many strain gages were placed on the wing structure to support real-time monitoring of component loads relative to strength limits. The load calibration test [5] used to calibrate these gages was intentionally more elaborate than necessary for the basic calibration and was designed to provide a broad database for parametric study.

2 Nomenclature

AAW	Active Aeroelastic Wing
CKCS	check-case
DLL	design limit load
EQDE	EQuation DErivation; in-house linear regression analysis package
NASA	National Aeronautics and Space Administration
rms	root mean square
TLL	test limit load

3 Analysis

3.1 Strain-Gage Instrumentation

The analysis method used here is determined by the instrumentation available on the AAW test aircraft. Figure 2 shows the location of the 20 component load measurement reference stations. The research reported here only examines the right-wing-root shear, bending moment, and torque; and the right-wing-fold shear, bending moment, and torque. Figure 3 shows the locations of the strain-gage instrumentation on the aircraft structure. Each strain-gage bridge is configured as a four-active-arm Wheatstone bridge. The wing structure includes seven spars in the inboard wing and six spars in the outboard wing. The wing design has a low aspect ratio and has highly redundant load paths. Additionally, a wing fold interrupts the spanwise load paths. These features make the F/A-18 wing a challenging structure for the derivation of good load equations. The wing-box strain-gage bridges were installed on the wing-root attach lugs, the wing skin, and on the webs of some of the spars as well as the wing-shear ties. Much of the strain-gage installation design here follows the pattern of previous F/A-18 loads aircraft practice. The 32 strain-gage bridges at wing station 65, however, were added specifically for strain-gage calibration research. A total of 158 strain-gage bridges were present on the left and right wing boxes.

3.2 Load Tests

The analysis method is also determined by the ground-loading test approach. Figure 4 shows the 16 load zones for the left wing. Each load zone was served by one load column comprised of a hydraulic cylinder, a load cell to measure the applied load, and a whiffletree mechanism to distribute the load to two, three, or four load pads. A total of 104 load pads were bonded to the lower surface of the wings to allow both tension and compression loading. These pads covered approximately 60 percent of the lower wing surface. Left and right wing loads were mirror images of each other, and the aircraft was always symmetrically loaded. A wide range of single-point- (one load zone per wing), double-point- (two load zones per wing), and distributed-load (16 load zones per wing) cases were performed. The total number of load cases

was 72. The maximum net vertical load exceeded four times the gross weight of the aircraft during distributed loading. Figure 5 shows the aircraft in ground test undergoing a distributed-load case. All load zones are active in this photo. Figure 6 shows a typical single-point load application. In this photo, load zone 16 is active while all the other load columns are disconnected. The bonded-on load pads and whiffletrees produced a tare weight effect because of their structural deadweight. This effect was transparent to the calibration process, as it was a constant force throughout each load run. Figures 7a and 7b show the wing-root bending moment and torque envelope with the single-point and distributed applied test loads. In these figures the notations S1 and D1 refer, respectively, to the single-point and distributed-load cases. The maximum test loads went to about 70 percent of flight design limit load [DLL] for the distributed loading. Figure 7a shows the small amount of the load envelope exercised by the single-point loading. Load cells were carefully calibrated and applied-load data and strain-gage data were recorded with 14-bit resolution. The actual load pad and hydraulic jack locations were determined using a three-head-sending theodolite measurement system. These processes provided for determining applied loads and moments with excellent precision. Reference 5 gives further details.

3.3 Load Equation Derivation

Strain-gage load equations were derived from selected subsets of the available recorded test data using an in-house linear regression analysis package called EQuation DErivation, or EQDE. Utilizing a modern desktop computer, EQDE derives the coefficients for user-selected combinations of strain-gage bridges based on analysis of the user-input test data. These test data consist of recorded measured applied loads and the corresponding strain-gage outputs. EQDE also automatically derives load equations for all possible strain-gage combinations from the input data. For example, if the user inputs test data from 20 strain-gage bridges, the software can be used to generate load equations for all possible combinations of two, three, four, and five strain-gage bridges. This thorough approach is termed an “exhaustive search” and is possible because of the computing speed of modern computers. No longer does the user need to judiciously select a limited number of strain-gage combinations as recommended in reference 1. It is always prudent, however, for the user to understand the reasonableness of the product of any software.

3.4 Load Equation Evaluation

EQDE also computes the root mean square [rms] of the fit of the derived load equation to the test data from which it was derived. This EQDE rms evaluation provides a quantitative metric indicating how well the derived equations represent the test data used in their derivation. EQDE ranks the order of derived load equations based on this computed rms so that the user need only consider the best of perhaps thousands of prepared equations. This research effort uses the EQDE rms as one metric of load equation quality. Of the 72 total load cases, 24 were fully distributed, utilizing 32 load zones simultaneously. Four of these distributed-load cases were set aside for use as an independent check case for the derived equations. These four load cases were excluded from use in the load equation derivation process. Figure 7c shows the four check-load cases, which are diverse, flight-like, independent-load cases. For each load equation studied, the rms fit of the load equation to these four load cases was calculated. This check-case rms computation is used as the second metric of equation quality. This second metric indicates how well the derived load equations can calculate loads for load cases from which they were not derived. This check-case rms therefore provides some additional insight into how well the load equations will perform with flight data. By deriving load equations from selected load cases, or parts of load cases, and then studying the resultant EQDE and check-case rms values,

one may observe the relative benefit of designing a load calibration test using only those load cases.

EQDE equation rms error =

$$\sqrt{\frac{\sum_{t=1}^{n}\left(\text{Derived load}_i - \text{Measured load}_i\right)^2}{\sum_{t=1}^{n}\left(\text{Measured load}_i\right)^2}} \quad (1)$$

Check-case equation rms error =

$$\sqrt{\frac{\sum_{t=1}^{n}\left(\text{Derived load}_i - \text{Check load}_i\right)^2}{\sum_{t=1}^{n}\left(\text{Check load}_i\right)^2}} \quad (2)$$

Figure 7d shows a graphical comparison of the measured applied test loads of distributed-load case B against outputs of two wing-root bending-moment equations, one derived from single-point loads and one derived from distributed loads. The outputs of each load equation were calculated using the strain-gage outputs that were recorded as these measured test loads were applied. The applied load curve is used as the truth model. If a load equation produces a line that closely fits the applied load curve, the indication is that this equation performs well in this part of the test load envelope. For a further comparison, the load equation outputs can be calculated and compared graphically against each of the four independent check cases. An equation that closely fits all four check cases can be expected to perform well throughout the entire flight envelope. The graphical comparison of a load equation with all four check cases can be replaced by a single numerical value when the rms of the differences is calculated. This is the check-case equation error defined above. Jenkins and Kuhl recognized the need for independent evaluation of derived load equations [6].

4 Results

4.1 Strain-Gage Location and Behavior Considerations

Figure 8 illustrates two types of strain-gage response to test load. The outputs of a wing-lug bridge and a nearby skin bridge are plotted against the applied load from a single-point load case on zone 7. The lug bridge has a very nonlinear response, while the skin bridge demonstrates linear behavior. If paired with another lug bridge that has a similar but opposite trend, the nonlinear lug bridge can still be useful. While both bridges can be effectively used in load equations, the lug-bridge representation is expected to suffer at low applied loads while the skin-bridge response can be readily captured even at relatively low applied test load. While this does demonstrate the broad variation possible amongst diverse instrumentation, the following trends are presented for potential application to the design of future load calibration tests.

4.2 Data-Conditioning Techniques

Test data used in these various parametric studies were filtered for noise spikes. In each case one increasing- and one decreasing-load test data segment was used. In some cases, data produced above a specified load level were excluded from the derivation input as noted, but even then the increasing- and decreasing-load data segments were both used. Data-conditioning was applied as uniformly as possible throughout so as not to introduce an artificial variation where one did not already exist.

4.3 Single-Point Compared With Distributed Loading

Figure 9a shows a comparison of the best two-, three-, four-, and five-gage wing-root-shear, bending-moment, and torque equations derived from single-point loading and from distributed loading. The check-case rms error for each

equation is plotted against its EQDE rms error. The most desirable area of the plot is low and left. A first observation is that allowing the inclusion of more gages generally improves the EQDE rms error and the check-case rms error. Figure 9b shows the same comparison but only for the four-gage equation results. This allows a less-cluttered comparison. The trend here is for the equations derived from distributed-loading test data to be better than those derived from the single-point loading test data. Figure 10 shows the same trend for wing-fold load equations. The better results produced by the distributed-loading database are the result of two merged features. While the obvious difference is that the distributed-loading cases involved all 16 load zones simultaneously as opposed to the one-zone-at-a-time process of the single-point loading, the distributed-loading cases produced much higher total net load than did the single-point loading cases. Figures 7a and 7b show the maximum net test load comparison between the single-point and distributed-load cases performed for this study. This emphasizes a typical limiting factor of single-point loading. When loads are introduced to the test structure through surface-contact load pads there is often a surface peak pressure limit, as required by local skin-bending or substructure-crushing considerations. Under these circumstances, the distributed-loading approach offers more total surface area than single-point loading can achieve. It is not possible to simply use a single huge load pad because of the high peak-to-average pressure ratio that would be produced by the combination of an elastic load pad in contact with an elastic wing. Similarly, there are practical limitations to the number of load pads one might want to accommodate. While the comparisons shown in figures 9 and 10 do not indicate the relative merit of these two features (load distribution and total load magnitude), they do clearly indicate the superior results produced by the net effect of the distributed-loading approach over the single-point loading scheme. It should be noted that reference 7 gives an example of a B-1 wing that was calibrated using both a distributed-load approach and a single-point load approach and concluded that there was very little difference in loads calculated from the two methods. The difference in the test load magnitude between single-point loading and distributed-loading, as indicated in figures 7a and 7b, is considered significant.

4.4 Test Load Magnitude Effect

This section presents the effect of varying the maximum applied load. Figure 11 shows the EQDE and check-case rms errors plotted against applied test load for four separate four-bridge wing-root bending-moment equations derived from the 16 single-point load cases. The effect of varying the peak magnitude of the applied test load was produced by selecting appropriate segments of the available load test data as input to EQDE. Separate load equations were derived for each increment of load, that is, 25, 50, 75, and 100 percent. Figures 12a and 12b graphically describe this approach. The 16 single-point load and strain-gage data sets were truncated at 25, 50, and 75 percent and used in addition to the full-range test data to vary the peak load magnitude. Wing-root bending moment was chosen from the six component loads to illustrate this trend. Wing-root bending moment is representative of the general trend of all data. Figure 11 shows a steady trend of slight improvement in the EQDE rms error for increasing load. With regard to check-case rms error, the same trend direction can be seen. This trend is not nearly as uniform, but shows a greater overall effect. One likely reason for the erratic check-case rms error trend is the considerable disparity in net applied test load magnitude between the single-point load cases and the distributed-load cases. This disparity is especially large when the single-point test data is truncated, as in this example. Remember that the check cases are a family of four distributed-load cases that reach 70 percent of the aircraft DLL. The extrapolation ratio involved in the use of load equations derived, from single-point test loading data truncated to 25 percent, to calculate these check-case loads is

about 10:1. If these equations were used with full-envelope flight data, the extrapolation ratio would be greater than 14:1. Another matter to keep in mind when considering the use of very small applied test loads is the presence of nonlinear gage responses, as shown in figure 8. The comparisons of the wing-fold-station bending-moment equations, which did not employ lug-mounted gages, were more linear.

Figure 13 shows the variation of the EQDE and check-case rms errors plotted against applied test load for four-gage wing-root bending-moment equations derived from 19 distributed-load cases. Here again, the effect of varying the magnitude of the maximum applied test load was produced by step-wise progressive truncation of the test data prior to equation derivation. This comparison, as with the single-point loading, shows a clear trend of improving EQDE rms error as applied test load is increased. This occurs in the check-case rms curves as well. The general improvement in accuracy is a factor of about two and one-half as the applied load increases by a factor of four. Although we are still concerned with nonlinear lug-mounted gages, the trends here show smaller nonlinearities than those produced by the single-point loading data. This is attributed to the greater overall applied loads produced by these distributed-load cases. The trends here indicate the diminishing benefit of the increasing applied load above 50 percent of applied test load. The EQDE rms error and the check-case rms error do not change linearly with the change in applied test load. While it has generally been thought that the best way to calibrate strain gages is to apply test loads equal to the maximum expected flight loads, here it can be understood that much of the benefit can be achieved by applying about half (75 percent DLL × 70 percent DLL) of the expected flight load. This obviously is influenced by the nonlinear nature of the structure–strain-gage installation combination. If one is able to assess the linearity of a planned test article relative to the F/A-18 wing used here, then one may consider this finding useful in designing loading for a calibration test.

4.5 Effect of Number of Load Cases

In order to examine the effect of the number of load cases on the quality of the derived load equations, a series of EQDE runs were made. The first run utilized the test data from all 16 single-point load cases as input. All of the load cases in this study went to 100 percent of test limit load [TLL] (represented in figure 7a). The second run utilized the data from only 15 of these test cases. Each subsequent derivation run dropped off one more load case data set until only the minimum number of cases was used. EQDE requires that there be equal or more load cases than the number of strain gages present in the derived load equations. The rms errors for the best four-gage wing-root bending-moment equations (based on the EQDE rms error values) that were produced from this study are reported in figure 14, plotted in order of increasing number of load cases. Table 1 shows the load case drop list. The order of this list was selected based on engineering judgment with the goal of gradually thinning the database. These load cases correspond to the load zones shown in figure 4 and the envelope loads shown in figure 7a. Figure 14 shows two general trends. As the number of included test cases is reduced the EQDE rms error trends downward, while the check-case curve eventually shows improvement in rms error magnitude. While the shapes of these curves are somewhat path-dependent—that is, they are related to the order in which the individual load cases were omitted—the trend shown here is that for this test- and load-case drop order, the most acceptable load equations were derived from 13 or more load cases. Please note that in the context of these low net load single-point load cases, the larger net load distributed-check-case rms errors are a stronger indicator of practical quality.

Table 1. Single-point load case attrition list.

Drop set number	Load case number
1	S16
2	S15
3	S14
4	S2
5	S12
6	S7
7	S8
8	S11
9	S13
10	S4

The same study of the effect of varying the number of load case data sets was performed within the context of distributed-loading tests. Figure 15 shows the EQDE rms and the check-case rms error curves for increasing numbers of distributed-loading cases. Table 2 shows the load case drop list; the load case envelope plot is given in figure 7b. Here again, the trend is that the EQDE rms error curve moves upward overall while the check-case rms error curve trends downward. The load equations that were used by the AAW project for safety-of-flight and research were generally derived using all available distributed-load case data. While, again, this is somewhat configuration-dependent, it is obvious that satisfactory load equations could be derived using anywhere from 6 to 19 diverse load cases. In fact, no significant benefit is indicated for the additional distributed-load cases beyond the minimum six used here. For this test, only six distributed-load cases produced results slightly better than the results produced by 13 single-point load cases. This is largely a function of the greater net load of the distributed-load cases. With regard to figure 15, the EQDE rms errors and the check-case rms errors carry equal credibility as they both are based on high-load data.

Table 2. Distribution-load case attrition list.

Drop set number	Load case number
1	D3
2	D20
3	D16
4	D22
5	D15
6	D21
7	D4
8	D10
9	D17
10	D23
11	D6
12	D12
13	D18
14	D1

4.6 Wing Surface Availability Effects

While it is most desirable to widely distribute the applied test loads at least in the aggregate if not in each load case, sometimes there are practical considerations that interfere with this. Surface-mounted instrumentation, imbedded sensors, or other fragile skin features may not permit contact pressures in the range of 20, 30, or higher psi as would otherwise be desired. Reference 7 includes a discussion of these types of restrictions in the load calibration of a B-2 wing. This section will address the effects on load equation rms errors of loading only the control surfaces or only the wing box. These issues were studied by segregating subsets of the single- and double-zone load test data sets and deriving load equations for each group of test data. Figure 16 shows a comparison of six sets of wing-root-shear load equations. The plot format is check-case rms error plotted against EQDE rms error with the best quality being low and left. The six load case sets are:

- single-zone loading on all wing zones (baseline),
- single-zone loading on the control surfaces only,
- single- and double-zone loading on the control surfaces only,
- single-zone loading on the wing box only,
- single- and dual-zone loading on the wing box only, and
- single- and dual-zone loading on the entire wing.

An observation is that there is some benefit produced with regard to check-case rms error by adding some dual-load cases, especially in the "wing-box-only" situation. It is interesting to note that it was possible to produce shear equations of similar quality to the baseline of "all single-point cases" using "control-surfaces single-point cases only" or "wing-box single- and dual-point cases."

Figure 17 shows wing-root bending-moment equation results derived from the same segregated test data sets. Here, the benefit of including dual-zoneloading cases is very evident between the two "control-surface-only" sets. Although this same benefit is not as evident between the two "wing-box-only" sets, they are at no disadvantage compared with the two "all-wing" sets. As with the shear equations example, it is noted that bending-moment equations of roughly equivalent quality can be produced using less than the baseline of "all single-point cases."

Figure 18 shows the wing-root-torque equation results derived from the same segregated test data sets. Here, it is obvious that giving up the greater torque-arm length of the control surfaces is a big disadvantage as shown in the two "wing-box-only" sets. Both of the "control-surfaces-only" groups returned good results. This emphasizes the importance of control-surface loading to the generation of good wing-root-torque equations.

5 Summary and Conclusions

Various issues regarding the design of aircraft strain-gage calibration loading tests have been discussed in this paper including: single-point loading compared with distributed loading, test load magnitude, number of load cases, and wing surface availability for loading. The importance of understanding the linearity of the strain-gage location has been emphasized, as well as the importance of using independent flight-like load cases for interpreting equation quality. Within the scope of this research effort it has been concluded that the distributed-loading approach generally yields superior results when compared with those produced by the single-point loading approach. This effect has been shown to be a result of the much greater net load magnitude possible with the distributed-loading approach. The effect of load magnitude was studied separately and found to be significant, however, while this test applied a peak of 70 percent design limit load, it was found that similar results could have been produced at only 50 percent design limit load. Although the load equations selected for use in safety-of-flight and flight research were derived from two dozen distributed-load cases, this study has shown that satisfactory equations could have been derived using as few as six diverse distributed-load cases. It has been found that when dealing with the matter of some structure being off-limits to loads testing, wing-root-torque equation quality depends heavily on control-surface loading. Wing-root-shear equation quality sometimes improves with the addition of some dual-point load cases. It was further suggested that greater improvements might be produced if all available load zones were used to produce some large distributed-load cases. Wing-root bending-moment equation quality was maintained through either wing-box-only loading or control-surface-only loading. The use of a set of independent, diverse, flight-like distributed loads to check the quality of the derived load equations was found to be a valuable asset.

References

[1] Skopinski T H, Aiken W S Jr and Huston W B. *Calibration of strain-gage installations in aircraft structures for the measurement of flight loads.* NACA Report 1178, 1954.

[2] Dryden Flight Research Center, *Flight loads laboratory*. Last modified September 24, 2001. http://www.dfrc.nasa.gov/Research/Facilities/FLL/index.html Accessed April 8, 2004.

[3] Pendleton E, Griffin K E, Kehoe M W and Perry B. A flight research program for active aeroelastic wing technology. AIAA 96-1574. 1996.

[4] Pendleton E, Bessette D, Field P, Miller G and Griffin K. Active aeroelastic wing flight research program: technical program and model analytical development. *Journal of Aircraft*, Vol. 37, No. 4, pp. 554–561, 2000.

[5] Lokos W A, Olney C D, Chen T, Crawford N D, Stauf R, and Reichenbach E Y. *Strain gage loads calibration testing of the active aeroelastic wing F/A-18 aircraft.* NASA/TM-2002-210726, 2002.

[6] Jenkins J M and Kuhl A E. *A study of the effect of radical load distributions on calibrated strain gage load equations*. NASA TM 56047, 1977.

[7] Jenkins J M and DeAngelis V M. *A summary of numerous strain-gage load calibrations on aircraft wings and tails in a technology format.* NASA Technical Memorandum 4804, 1997.

Figures

EC02-0264-16

Fig. 1. AAW aircraft in flight.

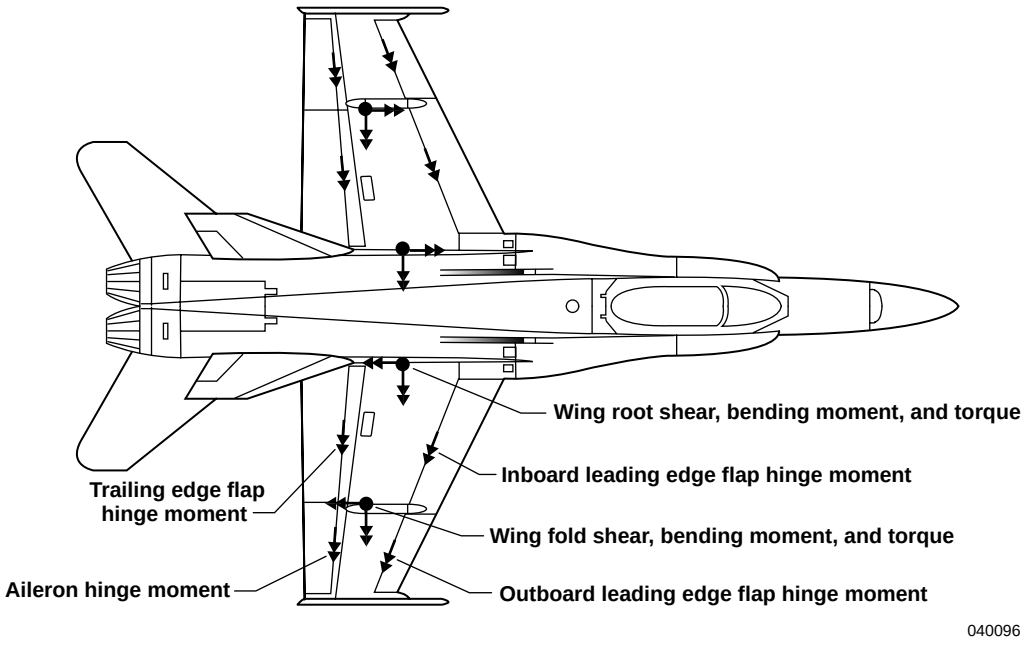

Fig. 2. Component load locations.

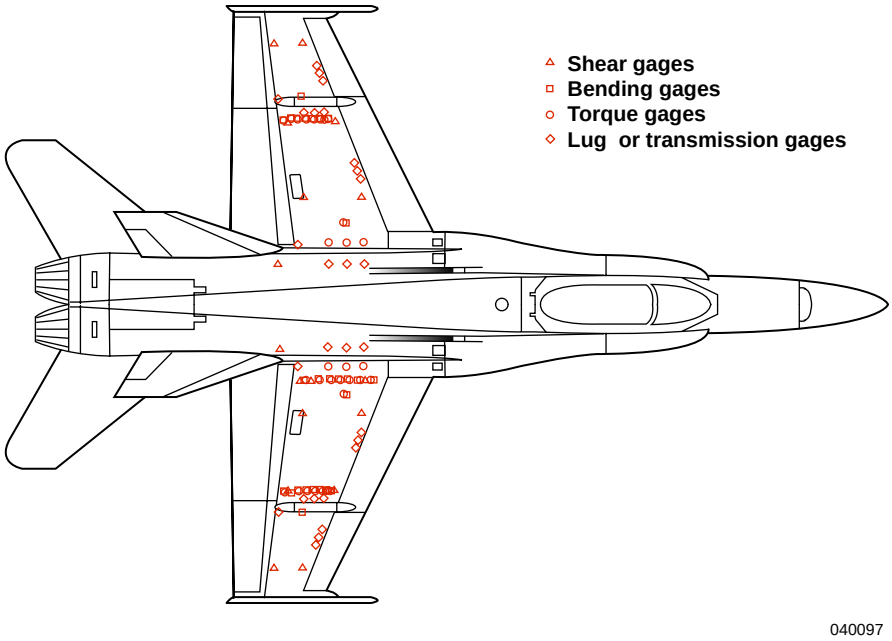

Fig. 3. Strain-gage bridge locations.

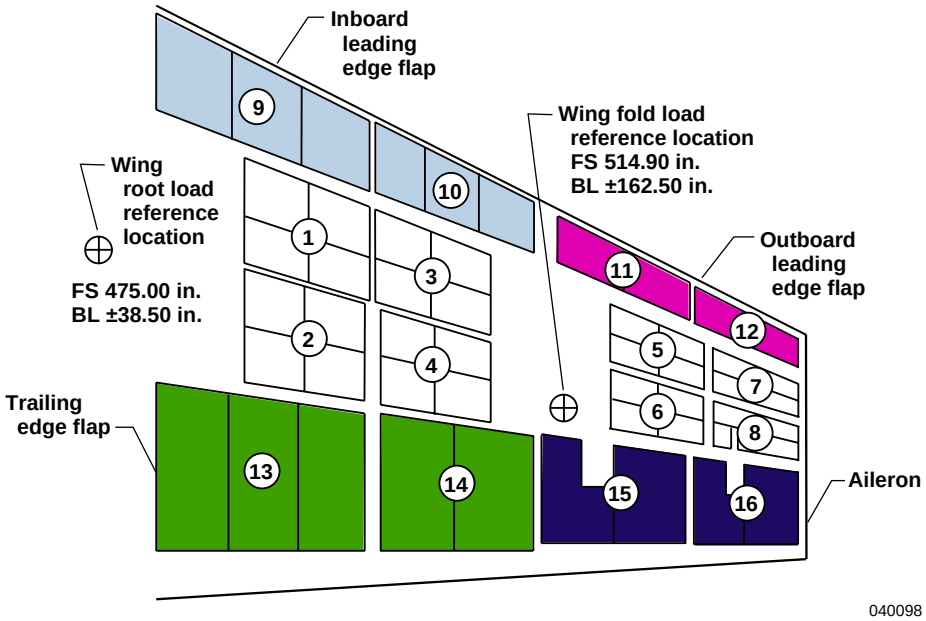

Fig. 4. Loading zones.

EC01-0249-06

Fig. 5. Composite photograph of AAW aircraft undergoing distributed loading at zero load and at maximum up load.

EC01-0249-52

Fig. 6. AAW aircraft in single-point loading (zone 16); right wing shown.

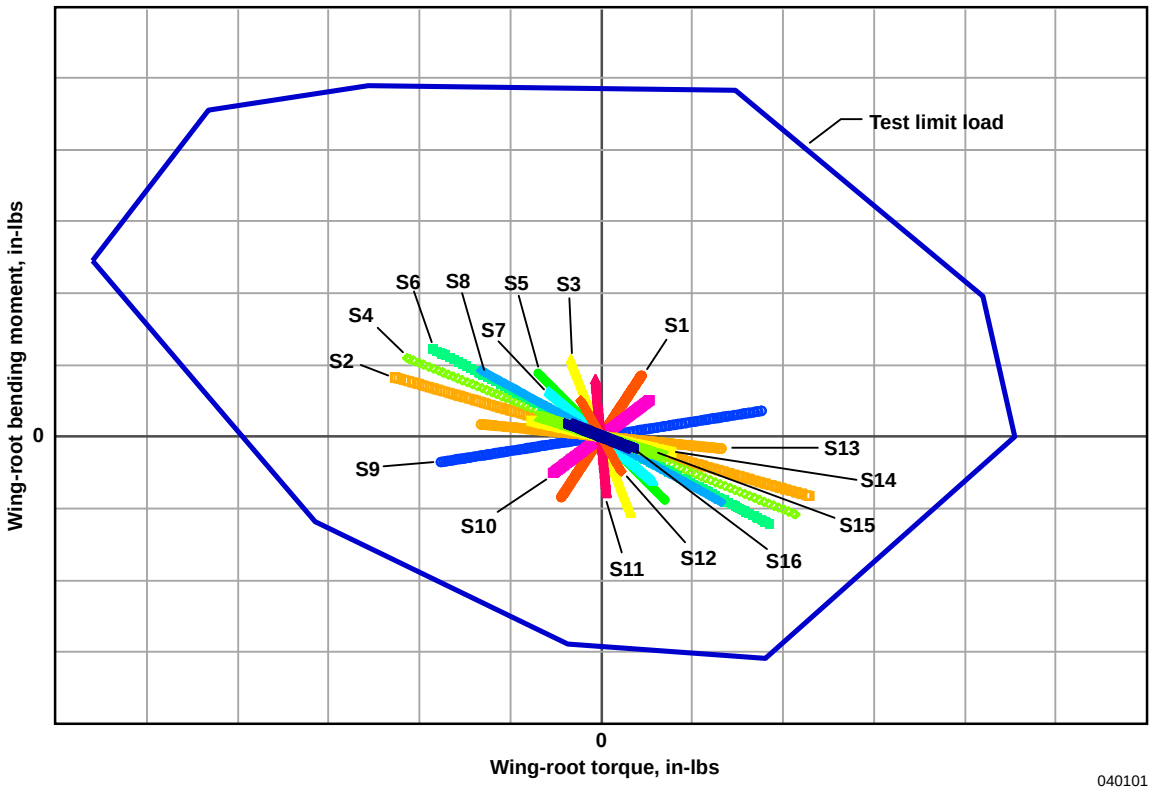

(a) Root bending–torque single-point load cases.

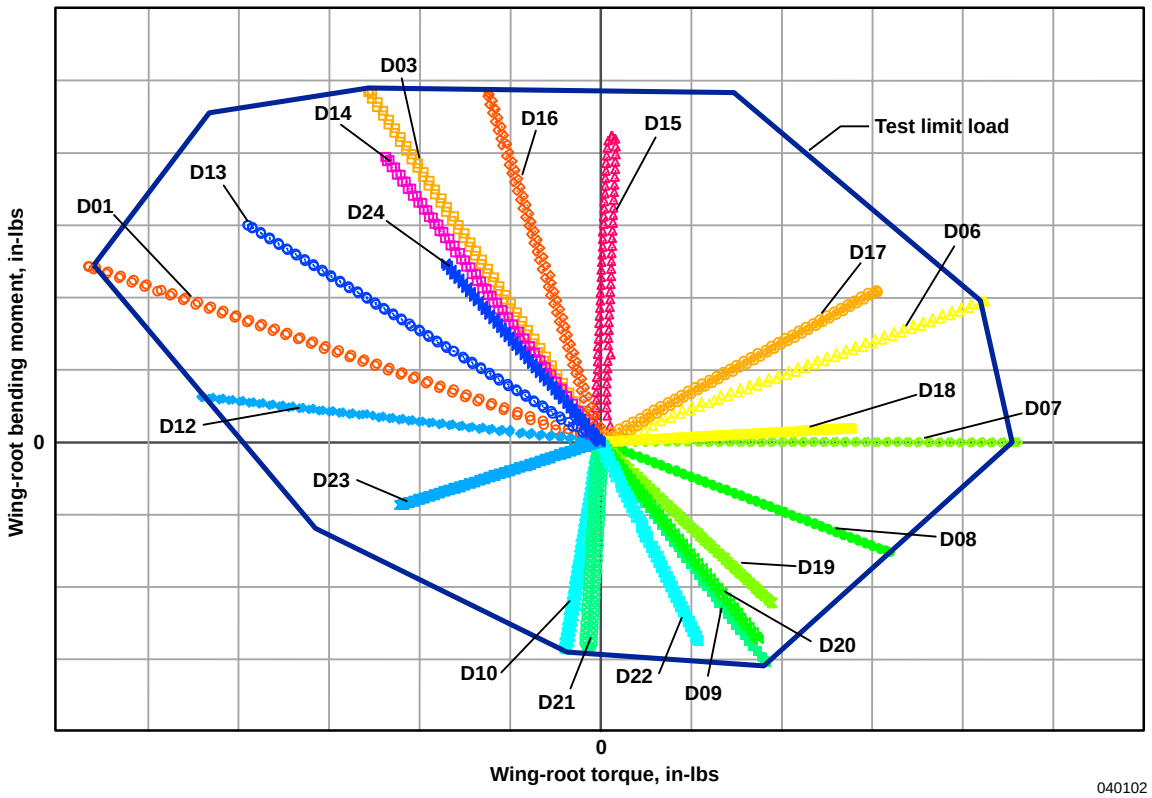

(b) Root bending–torque distributed-load cases.

Fig. 7. Load envelopes.

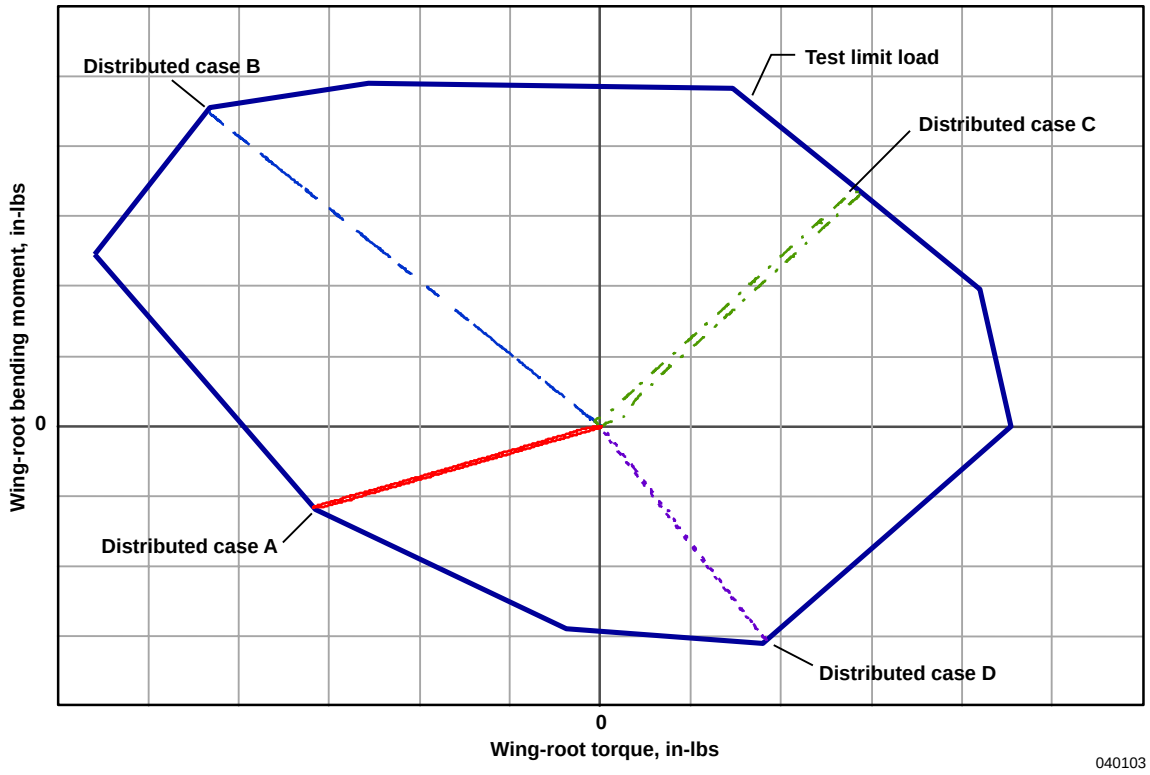

(c) Root bending–torque check-case distributed-load cases.

Fig. 7. Continued.

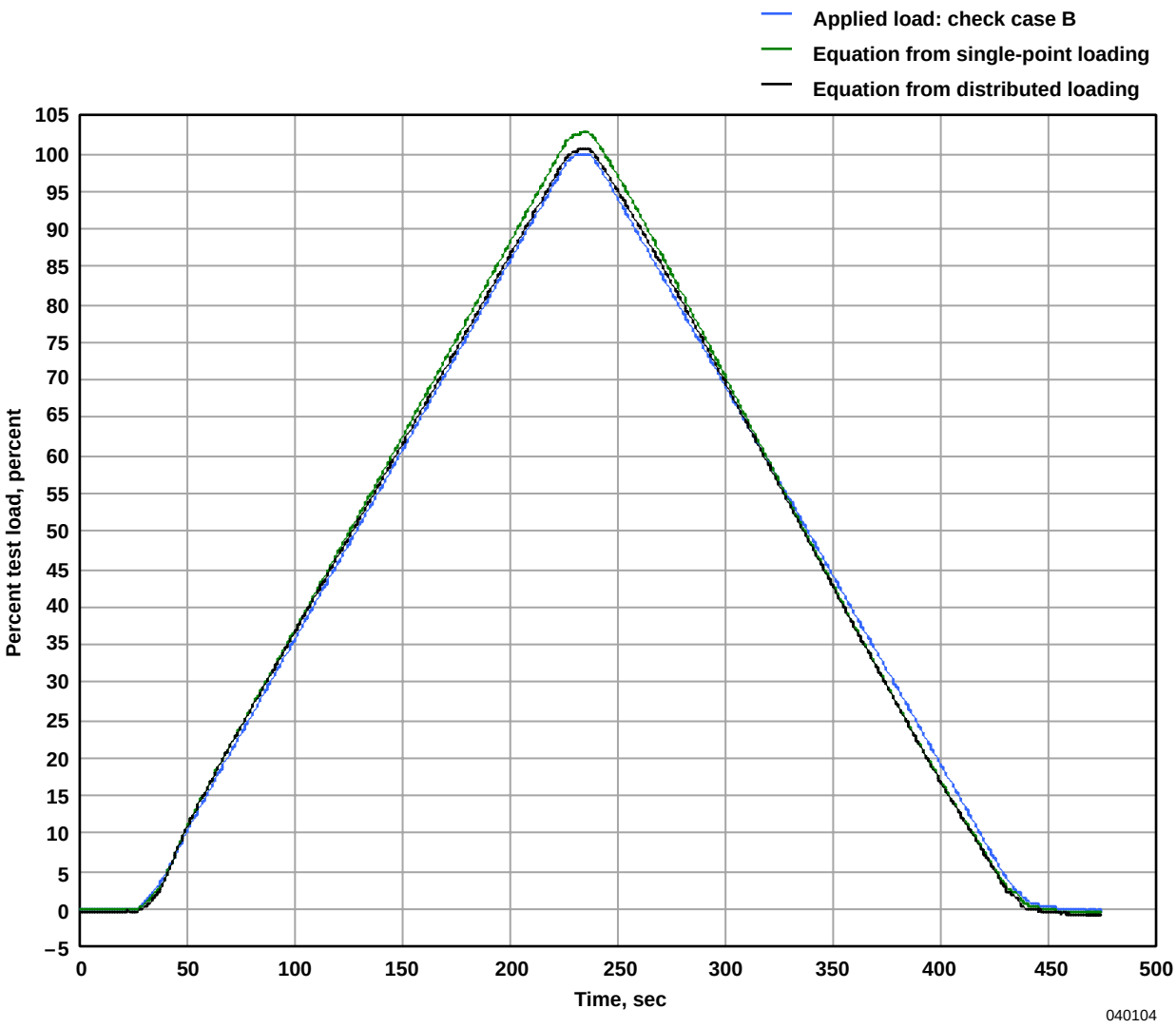

(d) AAW derived wing-root bending equations compared with applied load.

Fig. 7. Concluded.

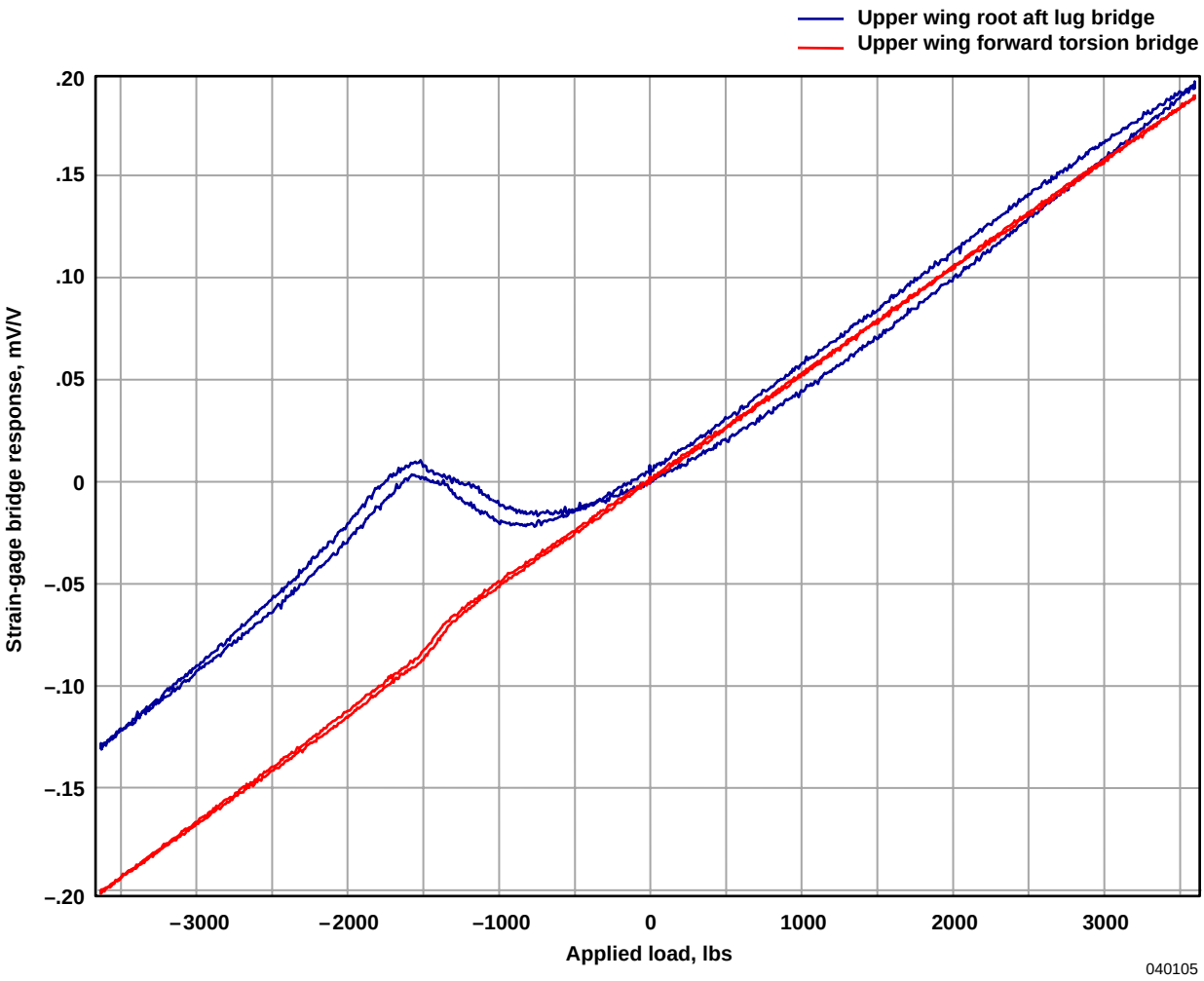

Fig. 8. Bridge output compared with load for a lug bridge and a skin bridge.

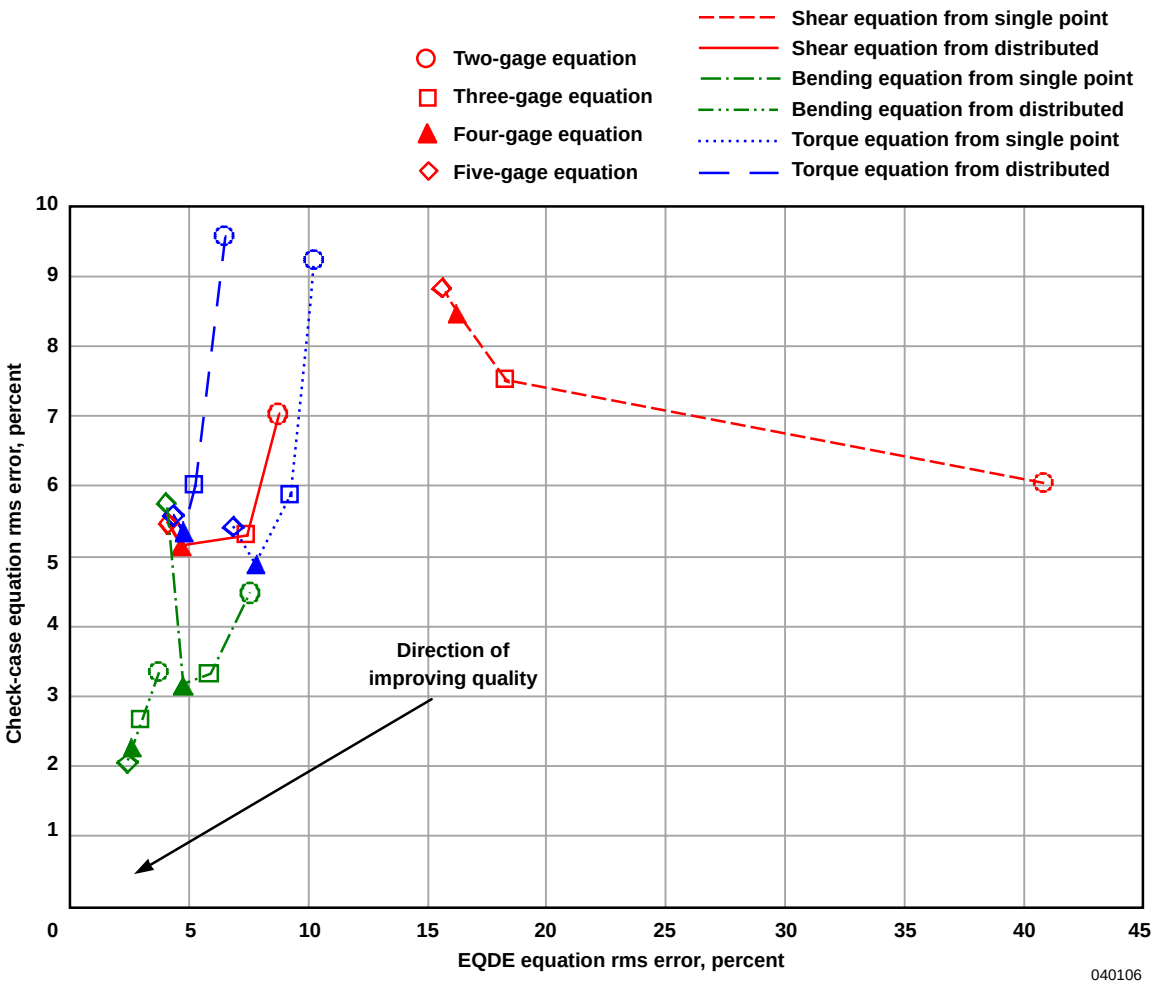

(a) Error comparison of best two-, three-, four-, and five-gage wing-root load equations derived from single-point and distributed-loading tests.

Fig. 9. Error comparisons.

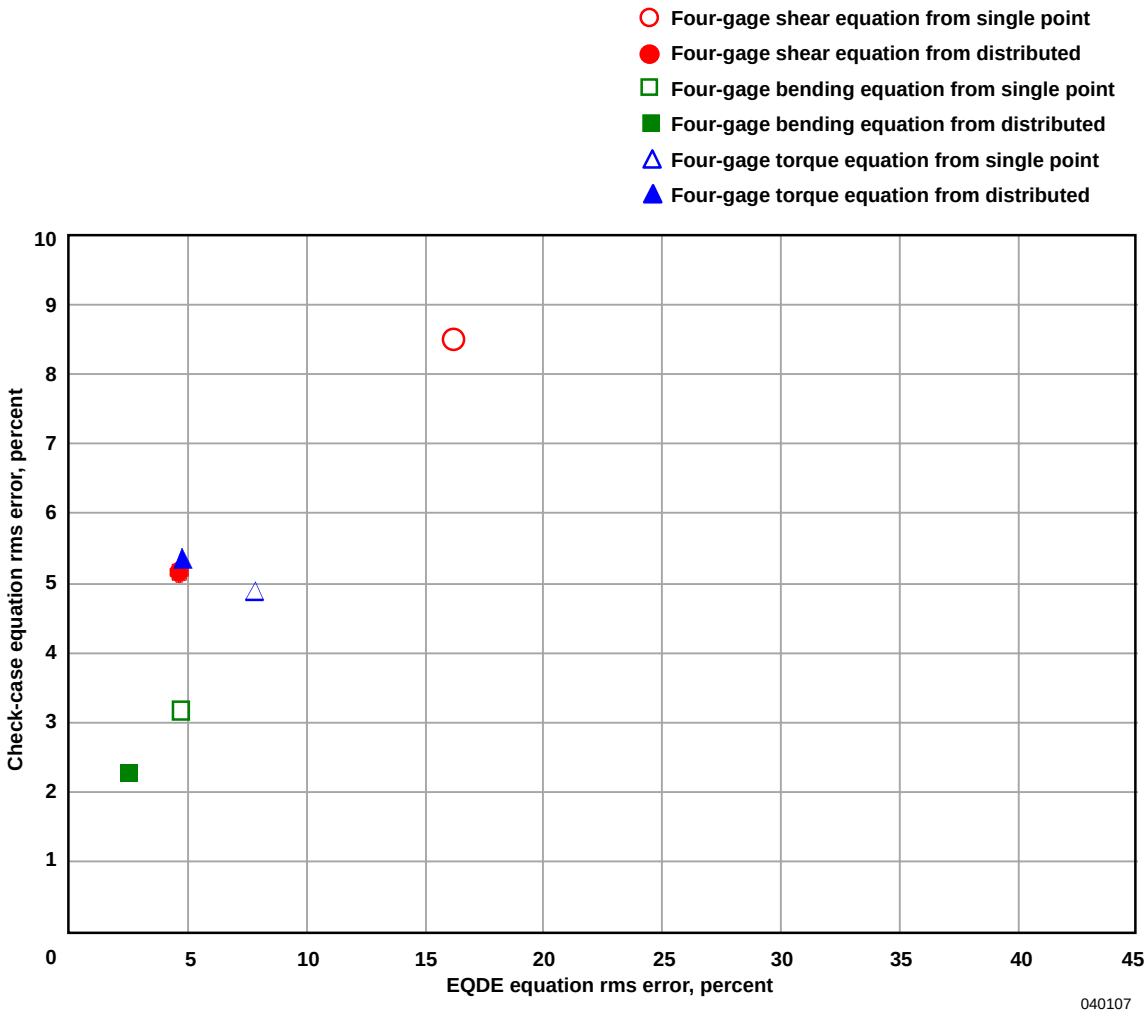

(b) Error comparison of best four-gage wing-root load equations derived from single-point and distributed-loading tests.

Fig. 9. Concluded.

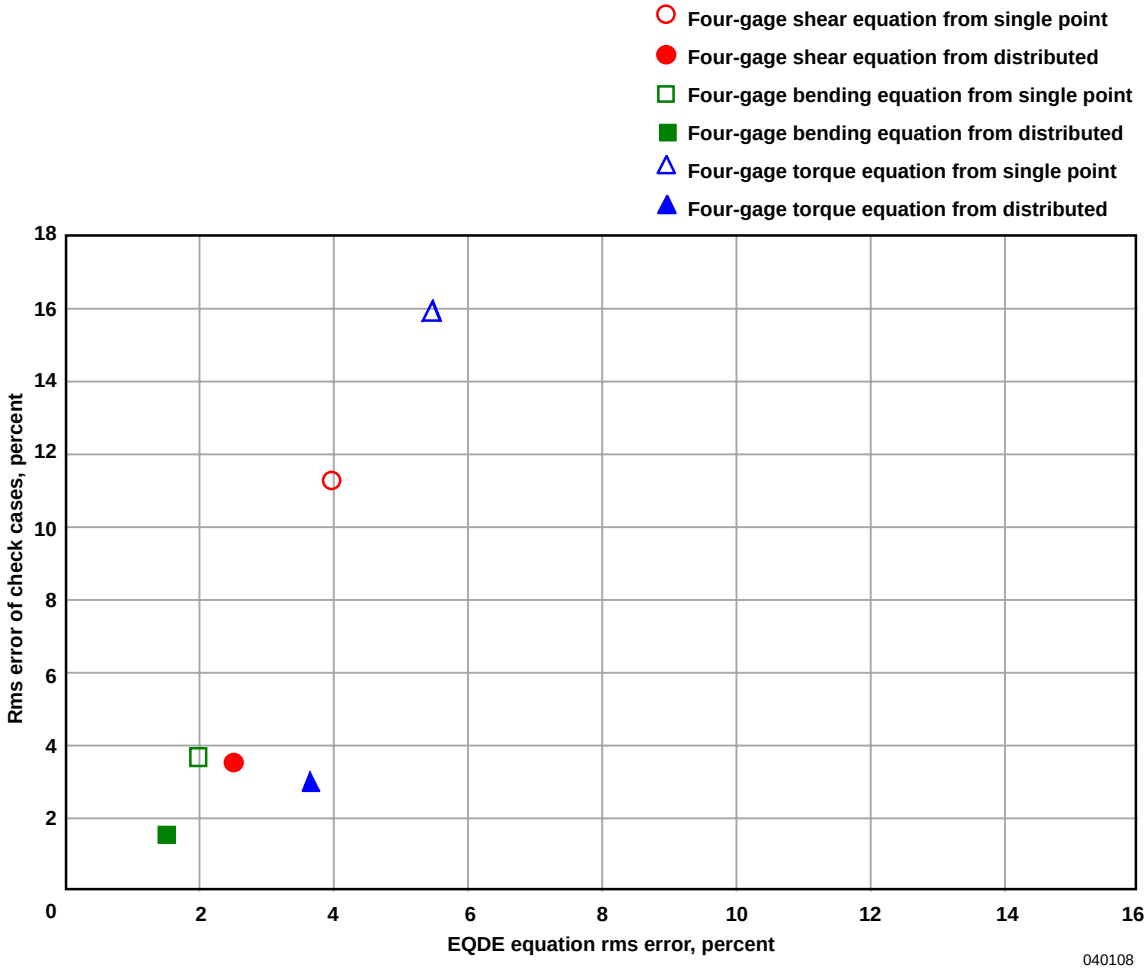

Fig. 10. Error comparison of wing-fold load equations derived from single-point and distributed-loading tests.

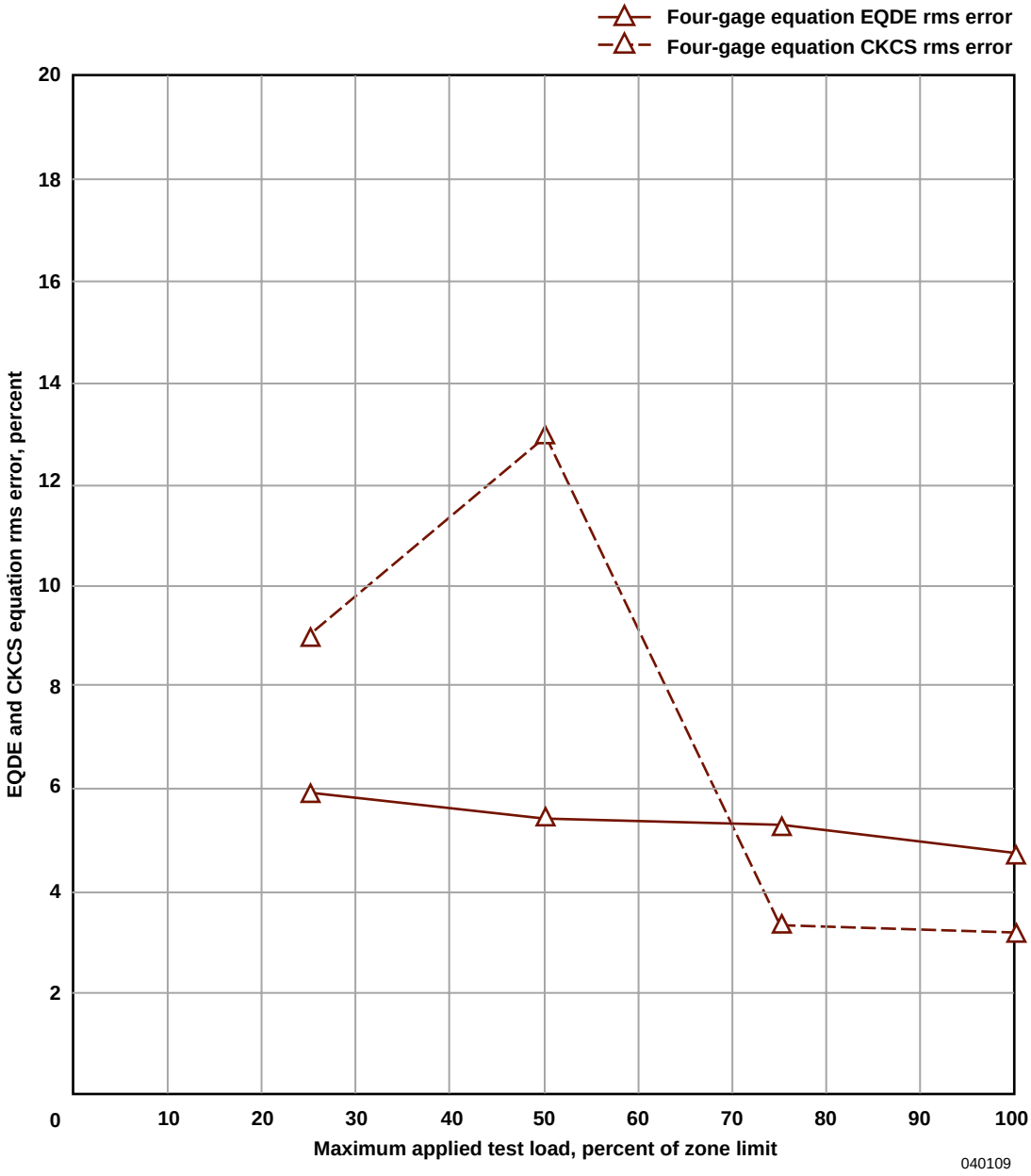

Fig. 11. Effect of variation of maximum test load on wing-root bending-moment equation errors (derived from single-point loading tests).

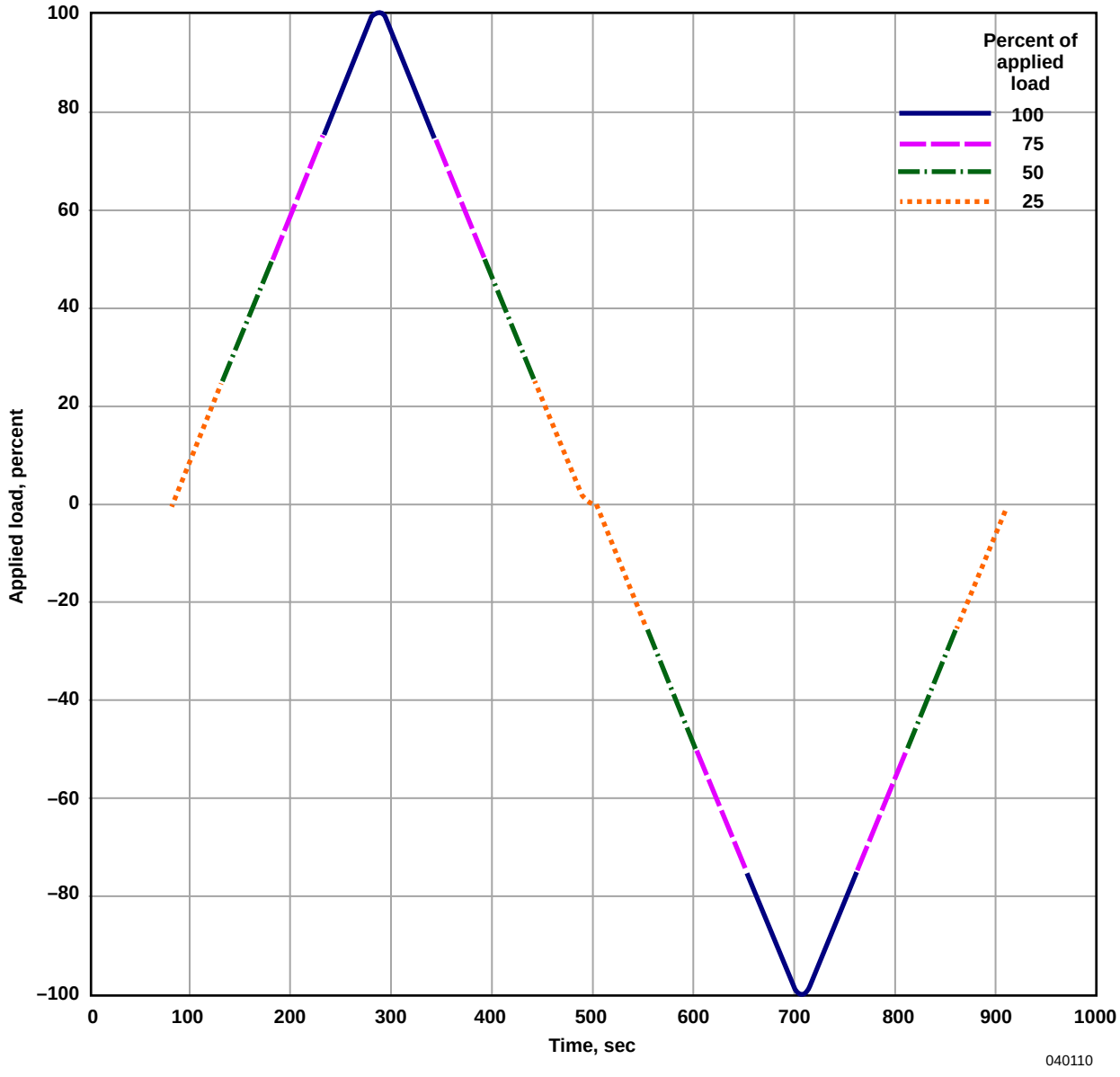

(a) AAW single-point load profile with percent load breaks.

Fig. 12. Load profiles.

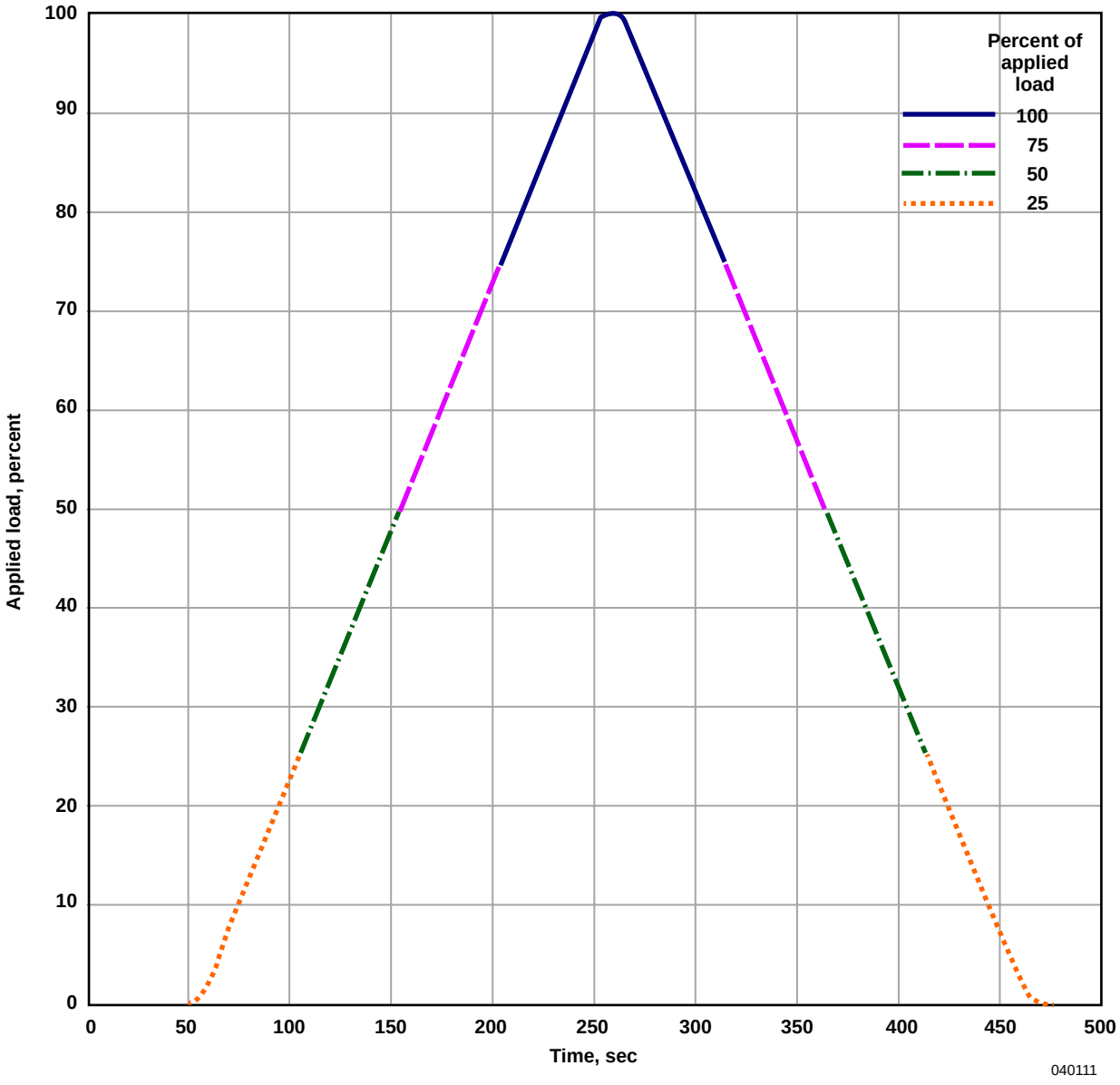

(b) AAW distributed-load profile with percent load breaks.

Fig. 12. Concluded.

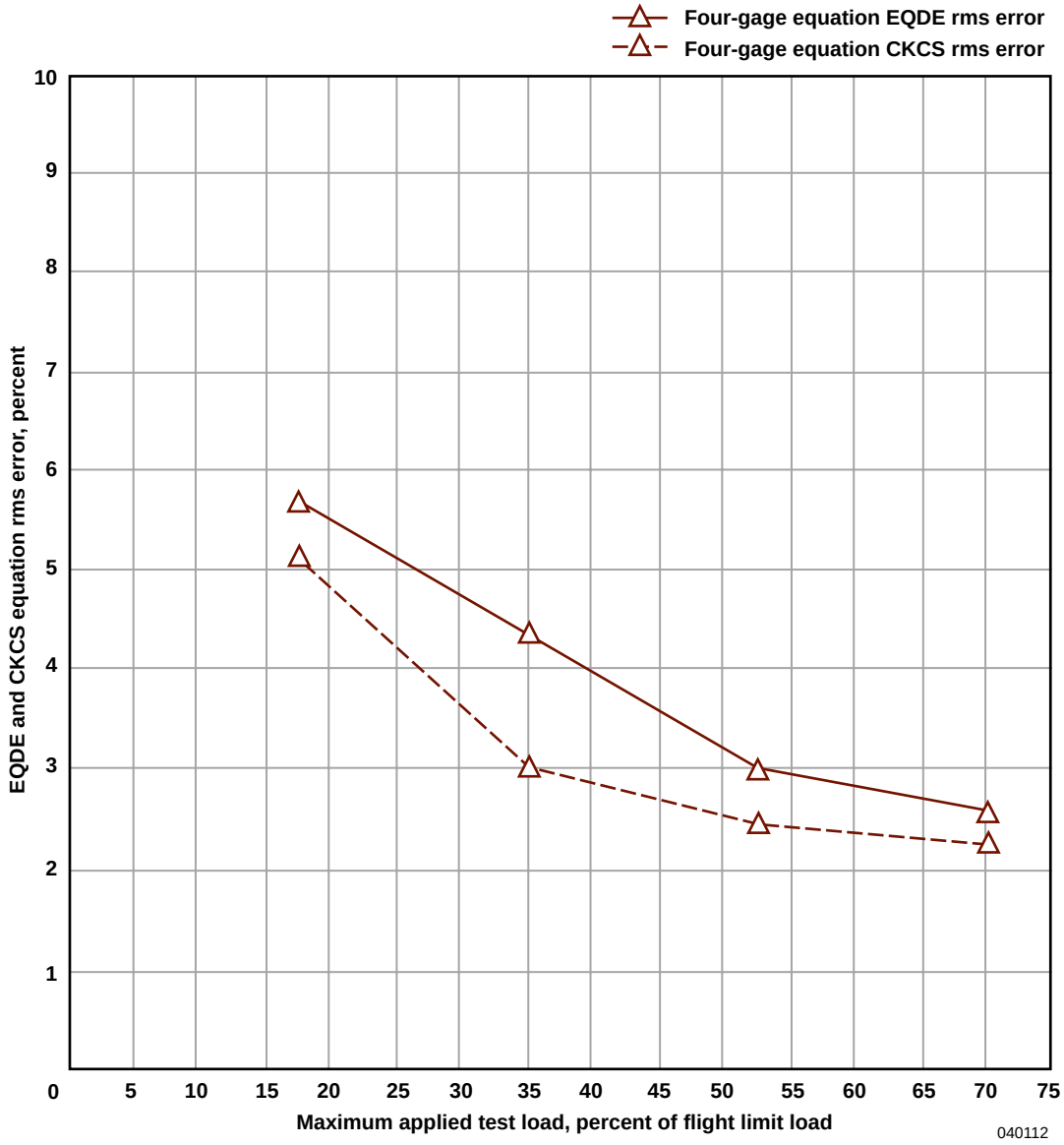

Fig. 13. Effect of variation of maximum test load on wing-root bending-moment equation errors (derived from distributed-loading tests).

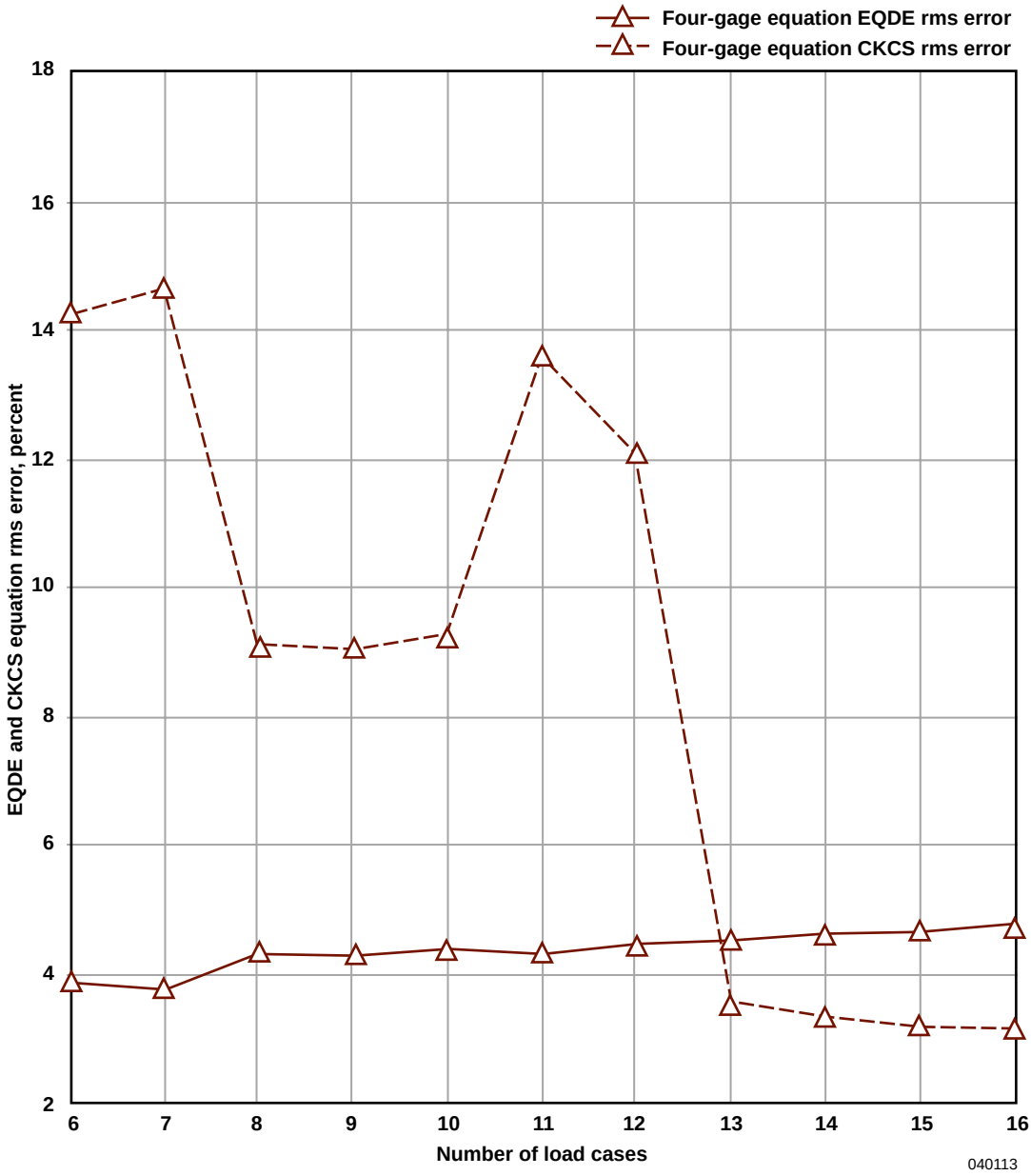

Fig. 14. Effect of number of single-point load cases used on wing-root bending-moment equation errors.

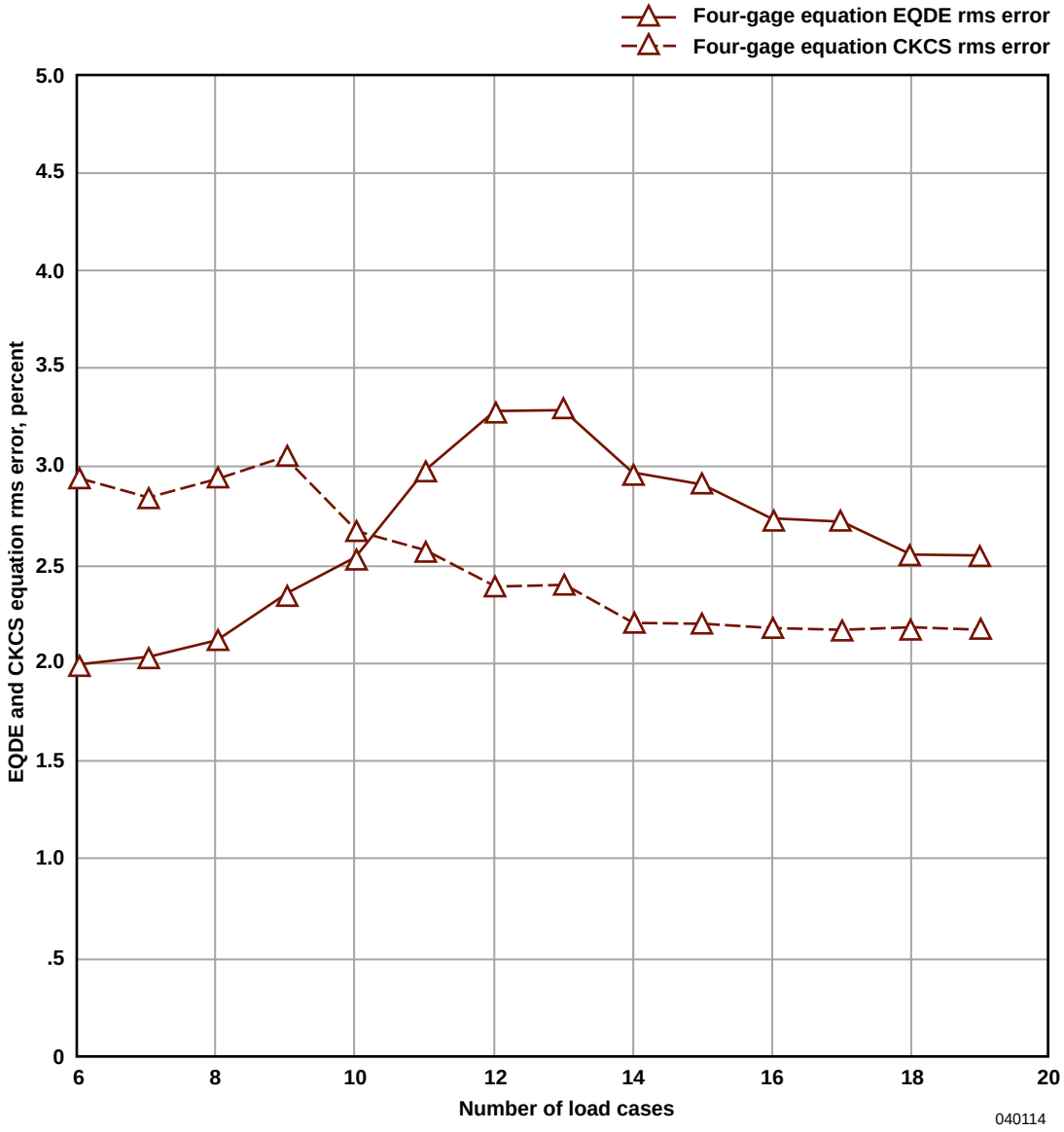

Figure 15. Effect of number of distributed-load cases used on wing-root bending-moment equation errors.

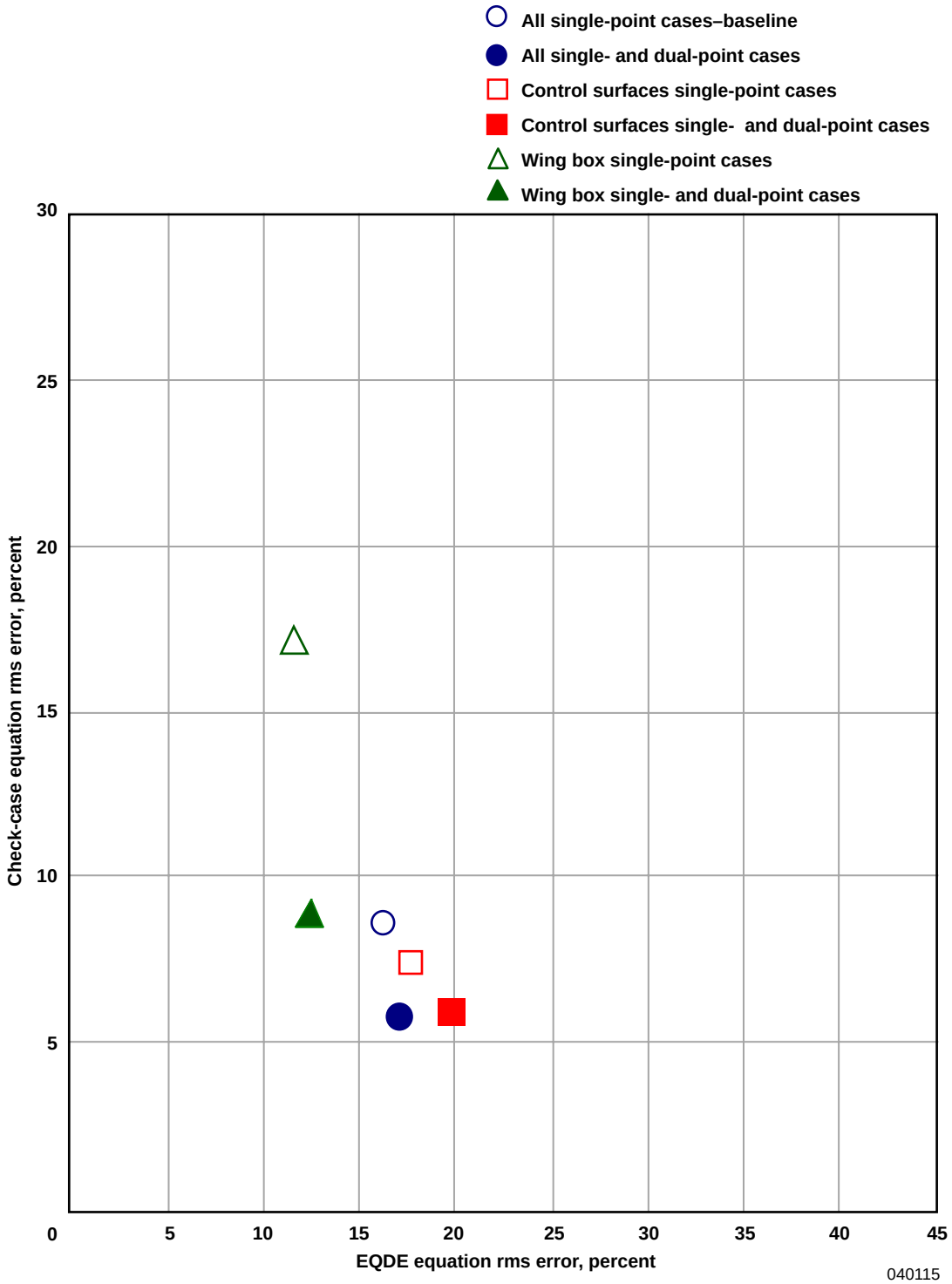

Figure 16. Effect of load zone availability and single- and double-zone loading on wing-root-shear rms errors.

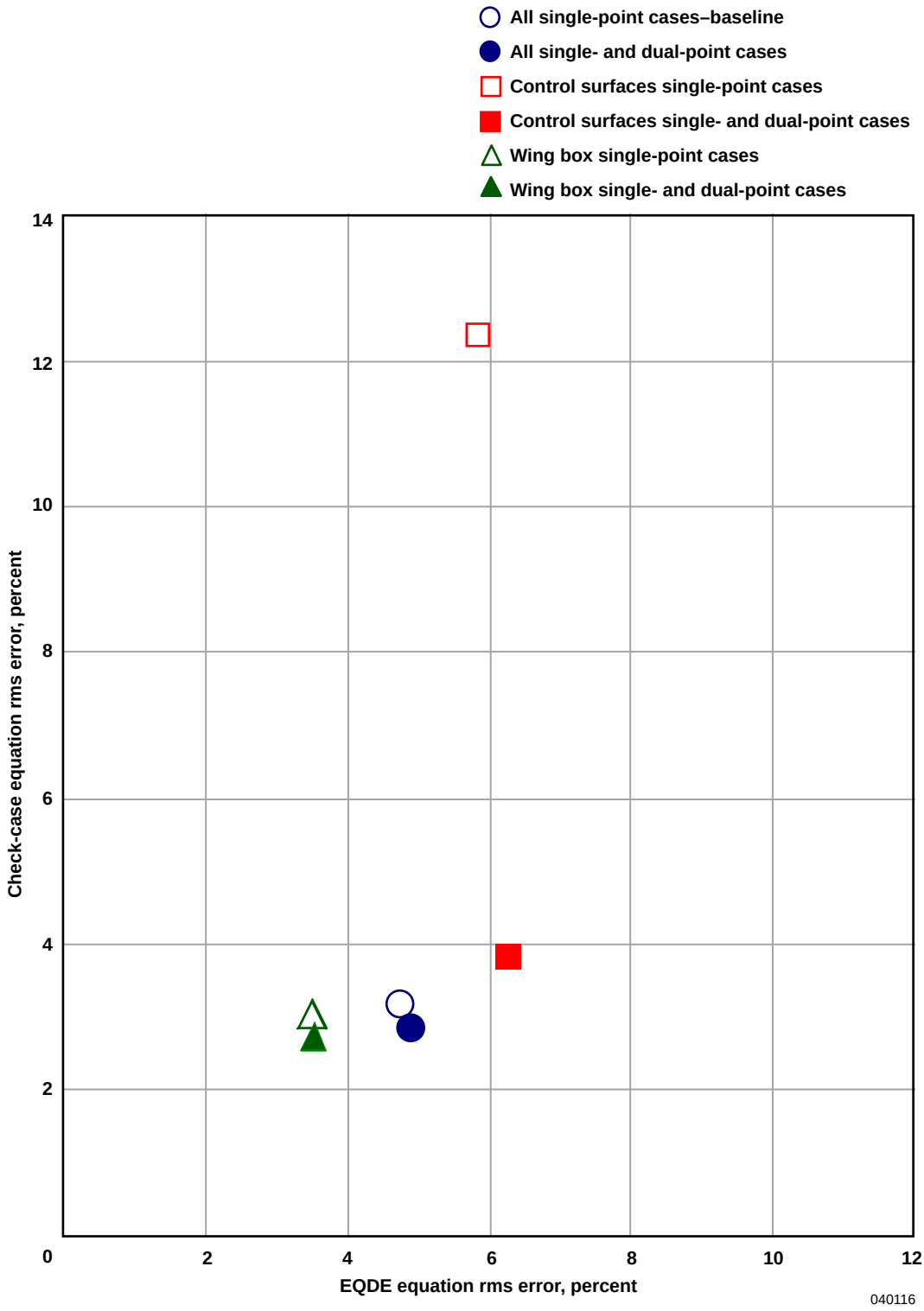

Figure 17. Effect of load zone availability and single- and double-zone loading on wing-root bending-moment rms errors.

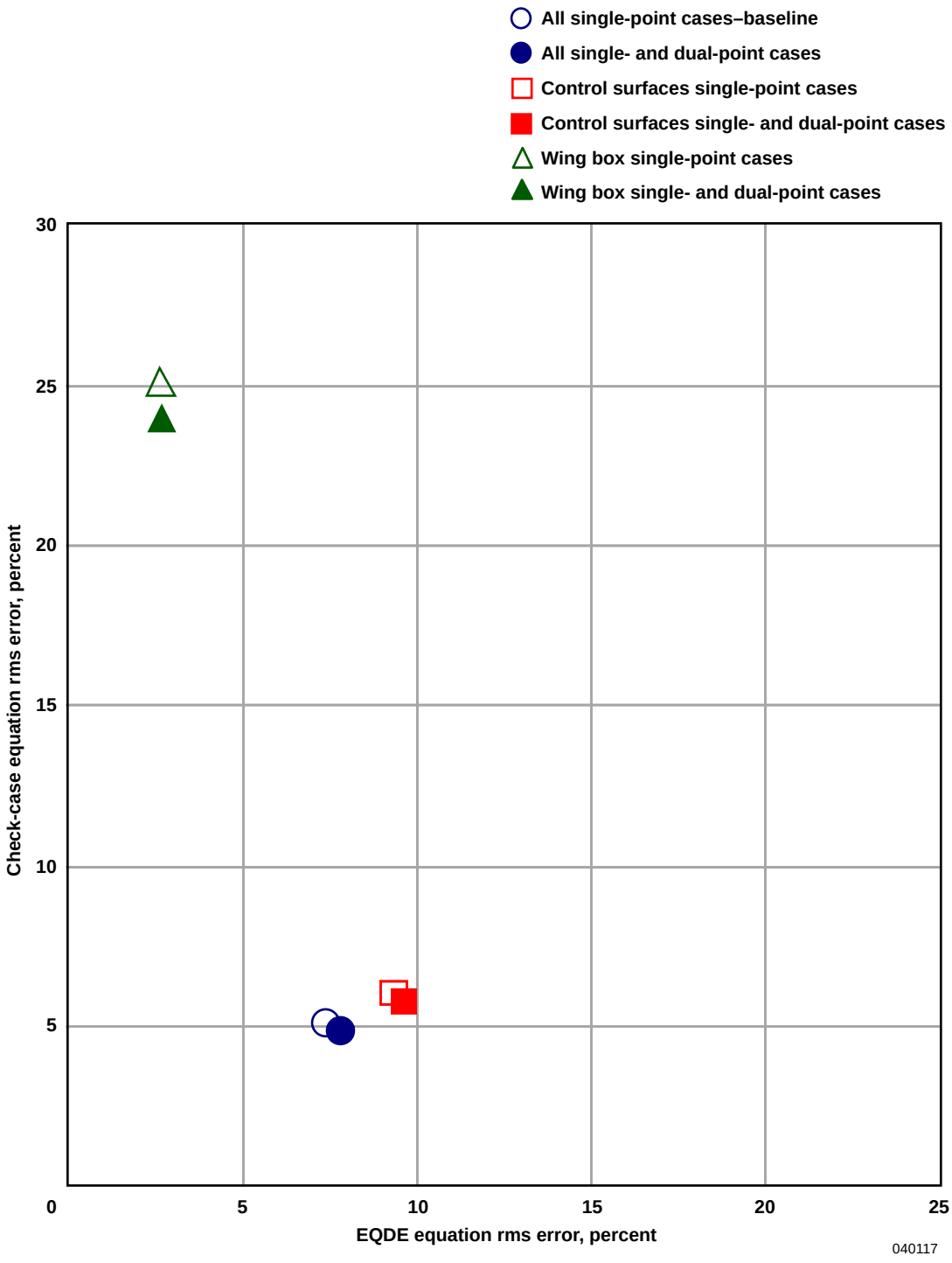

Figure 18. Effect of load zone availability and single- and double-zone loading on wing-root-torque rms errors.